Learning Patient-Specific Lumped Models
for Interactive Coronary Blood Flow Simulations

Hannes Nickisch[1], Yechiel Lamash[2], Sven Prevrhal[1], Moti Freiman[2],
Mani Vembar[3], Liran Goshen[2], and Holger Schmitt[1]

[1] Philips Research, Hamburg, Germany
[2] GRAD, CT, Philips Healthcare, Haifa, Israel
[3] Clinical Science, CT, Philips Healthcare, Cleveland, Ohio, USA

Abstract. We propose a parametric lumped model (LM) for fast patient-specific computational fluid dynamic simulations of blood flow in elongated vessel networks to alleviate the computational burden of 3D finite element (FE) simulations. We learn the coefficients balancing the local nonlinear hydraulic effects from a training set of precomputed FE simulations. Our LM yields pressure predictions accurate up to 2.76mmHg on 35 coronary trees obtained from 32 coronary computed tomography angiograms. We also observe a very good predictive performance on a validation set of 59 physiological measurements suggesting that FE simulations can be replaced by our LM. As LM predictions can be computed extremely fast, our approach paves the way to use a personalised interactive biophysical model with realtime feedback in clinical practice.

Keywords: CCTA, coronary blood flow, lumped parameter biophysical simulation, patient specific model.

1 Introduction

Fractional flow reserve (FFR) based on invasive coronary angiography is the gold-standard for the assessment of the functional impact of a lesion, thus helping
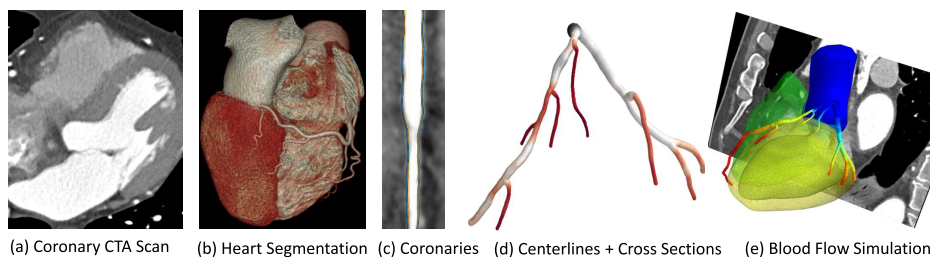

(a) Coronary CTA Scan   (b) Heart Segmentation   (c) Coronaries   (d) Centerlines + Cross Sections   (e) Blood Flow Simulation

Fig. 1. From image to simulation. The heart and its coronary arteries are (automatically) segmented from a CTA scan yielding a tree representation of centerline points and polygonal cross-sections (area encoded as color) used to conduct a patient-specific blood flow simulation (FFR encoded as color).
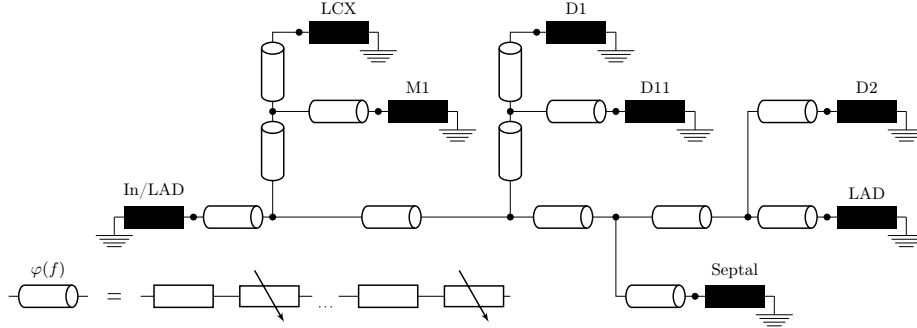
Fig. 2. Parametric nonlinear lumped model with $n = 21$ elements and $m = 15$ nodes including ground. Based on the centerline representation, we set up a lumped model with nonlinear resistances. The black boxes indicate inflow and outflow boundary conditions. The white tubes representing tree segment transfer functions $\varphi(f)$ are composed of a series of linear and nonlinear resistance elements reflecting both the local vessel geometry and hydraulic effects.

with clinical decisions for revascularization [14]. More recently, patient-specific simulations of physiologic information from the anatomic CCTA data have been proposed [7,16]. These computational fluid dynamics models are based on 3D finite element (FE) Navier-Stokes simulations, and are challenging both in terms of *computation* and *complexity*. Computation alone can be accelerated by performing them on GPUs, and complexity can be cut down by reduced order models e.g. [3,6,5], reuse of precomputations or lattice Boltzmann [10] methods. Operating a simulation pipeline from image to prediction (see Figure 1) in a failproof way is challenging as FE computations are sensitive to the quality of the underlying mesh. Besides complexity reduction, simpler and more robust models could be more appropriate for statistical reasons as many patient-specific parameters are unknown in practice. Lumped models (LM) were first used as systemic tree circulation model over 50 years ago [12] and later applied to the coronary circulation [9]. While machine learning techniques already assessed the sensitivity of a blood flow simulation to the segmentation [15], our goal is to use a data driven approach to approximate the FE simulation with a parametric LM that can be simulated extremely quickly. We determine the circumstances under which such an approximation is appropriate and accurate and use the LM for FFR predictions (Figure 1). The FFR value is defined as $FFR = P_d/P_a \in [0, 1]$ where P_d and P_a are the pressures distal and proximal to the stenosis averaged over the cardiac cycle. Values above 0.8 are regarded as insignificant [17], and repeated measurements have a standard deviation of $\sigma = 0.025$ [13] suggesting a grey zone of $0.8 \pm 2\sigma$ where clinical decisions require additional information.

2   Methodology

Most FE models use lumped boundary conditions such as Windkessels [20]; and their coupling is not always simple. As we are seeking a fast, simple and
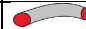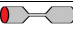
Hydraulic Effect	Geometry weights w_e, coefficients α_e and degrees d_e		Pictogram
1) Poiseuille friction	$w_P = 8\pi\mu\frac{\ell}{A^2}$	$d_P = 1$	
2) Expansion friction [18]	$w_E = \frac{\rho}{2}\max^2(0, \frac{1}{A_{in}} - \frac{1}{A_{out}})$	$d_E = 2$	
3) Ovality friction [11]	$w_O = w_P \cdot \left(\frac{P^2}{4\pi A}\right)^2$	$d_O = 1$	
4) Curvature friction [1]	$w_C = w_P \cdot \max\left(0, \frac{19}{8}(r\kappa)^{\frac{1}{25}} - 1\right)$	$d_C = 1$	
5) Bernoulli's principle	$w_B = \frac{\rho}{2}(\frac{1}{A^2} - \frac{1}{A_{out}^2})$	$d_B = 2$	
6) Bifurcation friction [19]	$w_{B_0} = \frac{\rho}{2A_{in}^2}$, $w_{B_1} = \frac{\rho}{2A_{out,1}^2}$, $w_{B_2} = \frac{\rho}{2A_{out,2}^2}$	$d_{B_0} = d_{B_1} = d_{B_2} = 2$	
Local effect superposition	$\varphi^c(f) = \sum_{e=1}^{E}\alpha_e\varphi_e^c(f)$	$= \alpha_1$ $+.. + \alpha_E$	
Tree segment compression	$\varphi(f) = \sum_{c=1}^{C}\varphi^c(f)$	$=$ $+$ $+$	

Fig. 3. Transfer functions and hydraulic effects. The geometry weights are obtained from the vessel's local cross-sectional area A, perimeter P, length ℓ, radius r and curvature κ. Blood density is denoted by ρ and viscosity by μ. Note that our cross-sections are not circular. Local effect-specific transfer functions $\varphi_e^c(f)$ are linearly combined to yield local transfer functions $\varphi^c(f)$. The local transfer functions $\varphi^c(f)$ are summed along the centerline $c = 1..C$ to yield the tree segment transfer function $\varphi(f)$.

parametrisable FE alternative, a lumped model is a natural choice. Using the hydraulic analogy, we can identify volumetric flow rate f with electrical current and pressure p with voltage allowing the interpretation of the coronary hydraulic network as an electrical circuit. Resistors translate into (constricted) pipes, current and voltage sources correspond to dynamic pumps. Starting from the tree representation shown in Figure 1(a), we set up a circuit with two macroscopic component types: nonlinear vessel segment resistors (white tubes) and boundary conditions (black boxes). The boundary condition may be a pressure or flow source driving the network; but any (lumped) boundary condition driving a conventional FE model can be used here. The challenge is to translate the local geometry of the vessel (radius, perimeter, cross-sectional area) into parameters of the nonlinear resistor. In the following, we detail our translation process.

2.1 Transfer Functions and Hydraulic Effects

The hydraulic analogon to Ohm's law is Poiseuille's law stating that pressure drop p and flow f through a thin elongated pipe are linearly related by the linear transfer function p_F so that $p = \varphi_P(f) = w_P f$, where the resistance constant w_P depends on the length of the pipe and its cross-sectional area. Poiseuille friction is only one *hydraulic effect* causing a pressure drop (or energy loss) in hydraulic networks. Friction between blood and the vessel wall is caused by changes of cross-sectional area, bifurcations as well as ovality and curvature of the vessel.

In our framework (see Figure 3), we use piecewise polynomial (invertable and point symmetric) *effect transfer functions* $\varphi_e^c(f) = w_e^c\mathrm{sign}(f)|f|^{d_e}$ to model hydraulic effects with degree d_e and geometry-specific weights w_e^c depending solely on the local vessel geometry and material constants such as blood density ρ and viscosity μ. If $d_e = 1$, we recover *resistors* and if $d_e \neq 1$, we talk about *varistors*. The functional form of the effect transfer functions were taken from the

fluid-mechanic literature [18,11,1,19] where the individual hydraulic effects had been experimentally and analytically studied in isolation. To combine multiple interdependent effects $e = 1..E$, we assume *local-effect superposition* $\varphi^c(f) = \sum_{e=1}^{E} \alpha_e \varphi_e^c(f)$ with *effect-specific coefficients* α_e. An illustration of local-effect superposition and tree segment compression is given at the bottom of Figure 3. In total, we include 6 different hydraulic effects, where the first 5 have a single coefficient each and the last one has three coefficients, yielding a total of 8 coefficients. To *compress* the size of the hydraulic network, we can sum up the transfer functions $\varphi^c(f)$ along a tree segment's centerline $c = 1..C$ into a single tree segment transfer function $\varphi(f) = \sum_{c=1}^{C} \varphi^c(f)$. This is possible because the flow through a tree segment is constant within the segment, as shown at the bottom of Figure 2. The compression operation can be inverted by *expansion*, once the simulation is done and the value of f is known. The hydraulic effects are also location specific in the sense that the first 5 effects are active everywhere except at bifurcations and the last one is active only at bifurcations. This representation of the hydraulic network as an assembly of transfer functions encoding hydraulic effects is now used to simulate blood flow.

2.2   Simulation

We make use of modified nodal analysis (MNA) [2] as employed in the popular circuit simulator SPICE[1]. A circuit graph is composed of $i = 1..m$ *nodes* and $j = 1..n$ *elements*. Note that $m < n$ since the circuit is connected. We wish to know the pressures p_j and flows f_j through all elements, a problem with $2n$ unknowns. In matrix-vector notation, we compute $\mathbf{p}, \mathbf{f} \in \mathbb{R}^n$ using *circuit topology* and *element properties* using the Newton-Raphson method. Typically, a handful of iterations are sufficient to solve the system up to machine precision which is due to two stepsize control mechanisms: damping and line search updates.

Topology. To impose Kirchhoff's laws (KL) on $\mathbf{p}$ and $\mathbf{f}$, MNA uses the (sparse) *node-to-element incidence matrix* $\mathbf{A}_0 = [a_{ij}]_{ij} \in \{\pm 1, 0\}^{m \times n}$ with $a_{ij} = 1$ if node i is input to element j, $a_{ij} = -1$ if node i is output to element j and $a_{ij} = 0$ otherwise. Selecting a ground node and removing the corresponding row yields the *reduced incidence matrix* $\mathbf{A} \in \{\pm 1, 0\}^{(m-1) \times n}$ allowing to express the KLs as $\mathbf{Af} = \mathbf{0}$ (conservation law) and $\mathbf{p} = \mathbf{A}^\top \mathbf{q}$ (uniqueness law) where $\mathbf{q} \in \mathbb{R}^{m-1}$ contains the *absolute pressures relative to the ground node*. Hence, we are left with $n + m - 1$ free variables in $[\mathbf{f}; \mathbf{q}]$ instead of $2n$ variables in $[\mathbf{f}; \mathbf{p}]$ and have $m - 1$ additional constraints (one per node except ground) through $\mathbf{Af} = \mathbf{0}$ so that the remaining number of degrees of freedom is n.

Element Properties. As a next step, we deal with the n remaining degrees of freedom by using the properties of the $n_R + n_P + n_F + n_V = n$ elements. We decompose $\mathbf{0} = \mathbf{Af} = \mathbf{A}_R \mathbf{f}_R + \mathbf{A}_P \mathbf{f}_P + \mathbf{A}_F \mathbf{f}_F + \mathbf{A}_V \mathbf{f}_V$ into its constituents (resistors, pressure sources, flow sources, varistors). Using $\mathbf{f}_R = \mathbf{R}^{-1} \mathbf{p}_R$, $\mathbf{f}_F = \hat{\mathbf{f}}_F$,

---

[1] See http://www.eecs.berkeley.edu/Pubs/TechRpts/1973/22871.html.

$\mathbf{p}_P = \hat{\mathbf{p}}_P$, $\mathbf{f}_V = \boldsymbol{\varphi}^{-1}(\mathbf{p}_V)$, where $\mathbf{R}$ is the diagonal resistance matrix and $\hat{\mathbf{f}}_F, \hat{\mathbf{p}}_P$ are vectors containing the pressure/flow source parameters and $\boldsymbol{\varphi}^{-1}$ denotes the n_V inverse varistor transfer functions stacked into a vector, we obtain a system of $n_x = m - 1 + n_P$ nonlinear equations in the variables $\mathbf{x} = [\mathbf{q}; \mathbf{f}_P] \in \mathbb{R}^{n_x}$

$$\begin{bmatrix} \mathbf{A}_R \mathbf{R}^{-1} \mathbf{A}_R^\top \ \mathbf{A}_P \\ \mathbf{A}_P^\top & \mathbf{0} \end{bmatrix} \begin{bmatrix} \mathbf{q} \\ \mathbf{f}_P \end{bmatrix} = \begin{bmatrix} -\mathbf{A}_F \hat{\mathbf{f}}_F \\ \hat{\mathbf{p}}_P \end{bmatrix} + \begin{bmatrix} -\mathbf{A}_V \boldsymbol{\varphi}^{-1}(\mathbf{A}_V^\top \mathbf{q}) \\ \mathbf{0} \end{bmatrix}. \qquad (1)$$

2.3   Parameter Learning

In the following, we detail how we adapt the effect coefficient vector $\boldsymbol{\alpha}$ to minimise the quadratic distance between lumped model (LM) simulation results and a training set of precomputed 3D finite element (FE) simulations. The training set consists of flows $\mathbf{f}_i^{FE} \in \mathbb{R}^n$ through each of the n elements of the circuit and absolute pressures $\mathbf{q}_i^{FE} \in \mathbb{R}^M$ at every cross-section of the coronary tree. Note that $m < M$ since the former refers to the number of nodes in the compressed circuit as shown in Figure 2 and the latter to the number of nodes in the expanded circuit. We use the flow from the FE simulation $\mathbf{f}_i^{FE}$ to compute the lumped model pressure drop $\hat{\mathbf{p}}_i^{LM}$ as a sum over the contributions from the effects $e = 1..E$ and set the coefficients $\boldsymbol{\alpha}$ to make the absolute pressure of the FE simulation $\mathbf{q}_i^{FE}$ and the absolute pressure $\hat{\mathbf{q}}_i^{LM} = \mathbf{C}\hat{\mathbf{p}}_i^{LM}$ as predicted by the lumped model as similar as possible via nonnegative least squares [8]

$$\boldsymbol{\alpha}_* = \arg\min_{\boldsymbol{\alpha} \succeq \mathbf{0}} \sum_{i=1}^n \left\| \mathbf{q}_i^{FE} - \mathbf{C}\hat{\mathbf{p}}_i^{LM} \right\|^2, \ \hat{\mathbf{p}}_i^{LM} = \sum_{e=1}^E \alpha_e \boldsymbol{\varphi}_e(\mathbf{f}_i^{FE}). \qquad (2)$$

Here, the matrix $\mathbf{C}$ implements cumulative summation along the tree starting from the root to convert relative pressures $\mathbf{p}$ into absolute pressures $\mathbf{q}$. We use the nonnegativity constraint on the coefficients to discourage non-physical model behavior. Note that learning avoids running lumped simulations; we only employ transfer functions.

3   Experiments

In the following, we describe two cascaded evaluation experiments; the first reporting on how well finite element (FE) simulations can be predicted by lumped model (LM) simulations and the second explaining how well the LM approach is suited for the prediction of physiological FFR measurements.

We trained a model with $E = 8$ coefficients $\boldsymbol{\alpha}$ (see Figure 3) on a data set collected from 32 patients and containing 35 coronary trees (either left or right) using a 20-fold resampled equal split into training and test set to avoid overfitting and obtain sensitivities (runtime $\sim$2min). We performed a total of 350 FE simulations (runtime $\sim$20min each) on these datasets with 10 different biologically plausible inflows[2] per coronary tree and mapped the simulated pressure

---

[2] The 10 equispacedly sampled flow rates were automatically adjusted to yield physically valid pressure drops ranging from a few mmH to 100mmHg for the dataset.
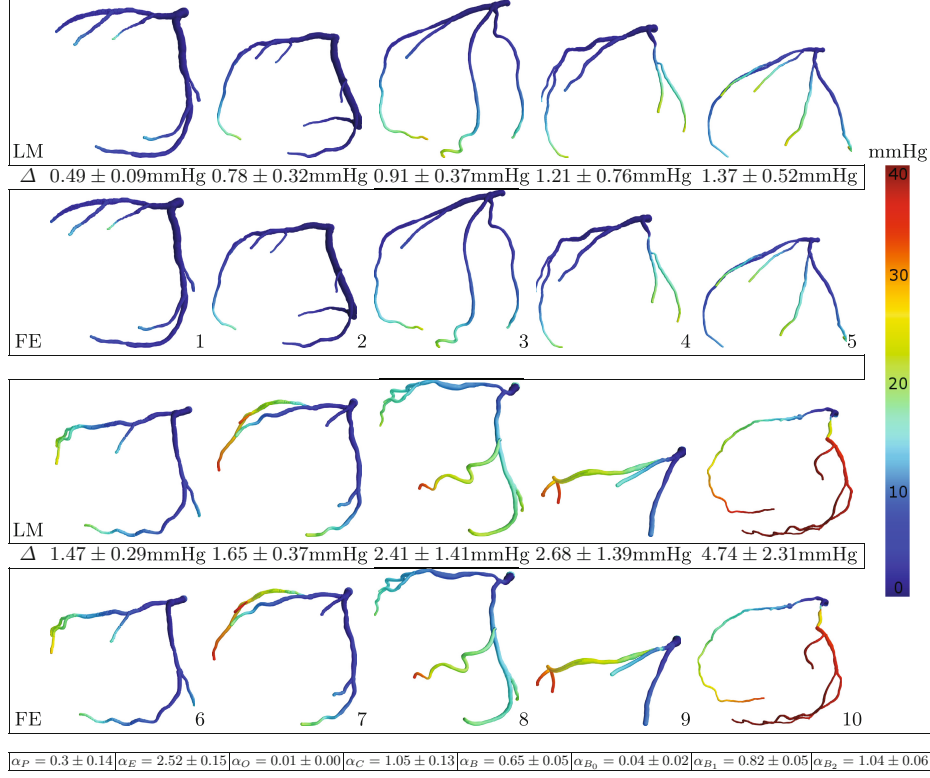
Fig. 4. Lumped model versus finite element simulations. We show LM simulated pressure drop $\mathbf{q}_{aorta} - \hat{\mathbf{q}}_i^{LM}$ and FE simulated pressure drop $\mathbf{q}_{aorta} - \mathbf{q}_i^{FE}$ for 10 exemplary coronary trees and measure their deviation Δ by the mean absolute error and its standard deviation averaged over the tree, 10 different flow rates and over the 20-fold resampling. We also report values for the coefficients $\boldsymbol{\alpha}$ along with standard error.

field and the velocity vector field on the centerline by averaging to generate the FE training data set consisting of volumetric flow rate $\mathbf{f}_i^{FE}$ and absolute pressure $\mathbf{q}_i^{FE}$ for every cross-section for the $i = 1..350$ runs. We used our own code for surface meshing and relied on Netgen[3] for volume meshing and OpenFOAM[4] to perform the calculations. From this dataset, leading to 10^5 terms in Equation 2, we computed the coefficient values as reported at the bottom of Figure 4 whose physical interpretation is hard. The predicted pressures in the 10 coronary trees of Figure 4 show a very good visual agreement and yield an average absolute deviation of 2.76mmHg±0.56mmHg.

We used another 41 patient data sets collected from multiple clinics with 59 FFR invasive measurements to benchmark our LM with the FE simulation on a clinical prediction task. As boundary conditions, for both models and left/right

---

[3] http://sourceforge.net/projects/netgen-mesher/

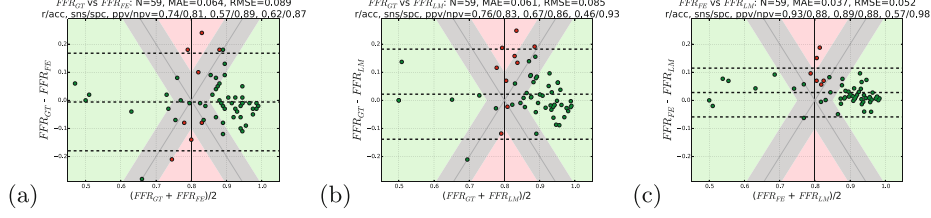[4] We use the FV solver simpleFoam from http://www.openfoam.com/.

Fig. 5. Comparison of lumped model (LM, runtime <1s) and finite element (FE, runtime 20min) FFR prediction with invasive ground truth (GT) measurements: We show using a Bland-Altman plot for all pairs (a) GT/FE, (b) GT/LM and (c) FE/LM to underpin the equivalence of LM and FE for this prediction task. The green and red color correspond to correctly or incorrectly classified datapoints according to the clinical threshold of 0.8. Gray is the intrinsic error margin. RMSE is the root mean squared error and MAE denotes the mean absolute error. Further, we report the correlation coefficient (r), the accuracy (acc), sensitivity (sns) and specificity (spc) as well as positive and negative predictive values (ppv,npv) for all pairs.

coronary trees independently, we employed an ostial pressure of $\hat{p} = 100$mmHg and outlet resistances R_i scaling with the outlet diameter d_i according to $R_i \propto d_i^{-1/3}$[4]. The result is summarised in Figure 5 showing similar performance for both FE (a) and LM (b) and a very good agreement between the two methods (c). The intrinsic error of $2\sigma = 0.05$ for a repeated FFR measurement [13] puts the dashed 2σ bands in Figures 5 (a)-(c) in perspective. The LM's accuracy and the deviation from the FE model are about the same.

4   Discussion and Conclusion

We have presented a steady-state parametric lumped model (LM) framework simulating FFR values with accuracy comparable to finite element (FE) simulations in a fraction of a second. The framework is extensible in at least three ways: 1) It is possible to envisage transient simulations by including capacitors or inductors. 2) Following this, one can directly use physiological measurements as training data instead of precomputed FE simulations. 3) Finally, derivatives w.r.t. transfer function parameters can be computed analytically by the implicit function theorem which sets the stage for learning boundary conditions directly from data. We have left open the question about the physical significance of the learned coefficients because the underlying hydraulic effects are not independent of each other. Instead, we prefer to regard the transfer functions of the hydraulic effects merely as *features* in a linear machine learning model. Our computations were based on CT images but other modalities such as interventional Xray can be targeted. We demonstrated comparable accuracy for both LM and FE models with deviations in the order of the ground truth variability; but even if LMs were not accurate enough for some cases, their simplicity and speed makes them a valuable interactive tool for segmentation guidance and quick estimation.

References

1. Ali, S.: Pressure drop correlations for flow through regular helical coil tubes. Fluid Dynamics Research 28(4), 295–310 (2001)
2. Ho, C.-W., Ruehli, A.E., Brennan, P.A.: The modified nodal approach to network analysis. IEEE Transactions on Circuits and Systems 22(6), 504–509 (1975)
3. van der Horst, A., Boogaard, F.L., Rutten, M.C.M., van de Vosse, F.N.: A 1D wave propagation model of coronary flow in a beating heart. In: ASME Summer Bioengineering Conference (2011)
4. Huo, Y., Kassab, G.S.: Intraspecific scaling laws of vascular trees. Journal of the Royal So 9, 190–200 (2012)
5. Huo, Y., Svendsen, M., Choy, J.S., Zhang, Z.D., Kassab, G.S.: A validated predictive model of coronary fractional flow reserve. Journal of the Royal Society Interface 9(71), 1325–1338 (2012)
6. Itu, L., Sharma, P., Mihalef, V., Kamen, A., Suciu, C., Comaniciu, D.: A patient-specific reduced order model for coronary circulation. In: ISBI (2012)
7. Kim, H.J., Vignon-Clementel, E., Coogan, J.S., Figueroa, C.A., Jansen, K.E., Taylor, C.A.: Patient-specific modeling of blood flow and pressure in human coronary arteries. Annals of Biomedical Engineering 38(10), 3195–3209 (2010)
8. Lawson, C.L., Hanson, R.J.: Solving Least Squares Problems. SIAM (1987)
9. Maasrani, M., Abouliatim, I., Ruggieri, V., Corbineau, H., Verhoye, J.P., Drochon, A.: Simulations of fluxes in diseased coronary network using an electrical model. In: International Conference on Electrical Machines (ICEM) (2010)
10. Melchionna, S., Bernaschi, M., Succi, S., Rybicki, E.K.F.J., Mitsouras, D., Coskun, A.U., Feldman, C.L.: Hydrokinetic approach to large-scale cardiovascular blood flow. Computer Physics Communications 181(3), 462–472 (2010)
11. Muzychka, Y., Yovanovich, M.: Pressure drop in laminar developing flow in non-circular ducts: a scaling and modeling approach. J. of Fluids Engin. 131(11) (2009)
12. Noordergraaf, A., Verdouw, P.D., Boom, H.B.K.: The use of an analog computer in a circulation model. Progress in Cardiovascular Diseases 5(5), 419–439 (1963)
13. Petraco, R., Sen, S., Nijjer, S., Echavarria-Pinto, M., Escaned, J., Francis, D.P., Davies, J.E.: Fractional flow reserve–guided revascularization: practical implications of a diagnostic gray zone and measurement variability on clinical decisions. JACC: Cardiovascular Interventions 6(3), 222–225 (2013)
14. Pijls, N., van Son, J., Kirkeeide, R., Bruyne, B.D., Gould, K.L.: Experimental basis of determining maximum coronary, myocardial, and collateral blood flow by pressure measurements for assessing functional stenosis severity before and after percutaneous transluminal coronary angioplasty. Circulation 87, 1354–1367 (1993)
15. Sankaran, S., Grady, L.J., Taylor, C.A.: Real-time sensitivity analysis of blood flow simulations to lumen segmentation uncertainty. In: Golland, P., Hata, N., Barillot, C., Hornegger, J., Howe, R. (eds.) MICCAI 2014, Part II. LNCS, vol. 8674, pp. 1–8. Springer, Heidelberg (2014)
16. Taylor, C.A., Fonte, T.A., Min, J.K.: Computational fluid dynamics applied to cardiac computed tomography for noninvasive quantification of fractional flow reserve. Journal of the American College of Cardiology 61(22), 2233–2241 (2013)

17. Tonino, P., Bruyne, B.D., Pijls, N., Siebert, U., Ikeno, F., van't Veer, M., Klauss, V., Manoharan, G., Engstrøm, T., Oldroyd, K., Lee, P.V., MacCarthy, P., Fearon, W.: Fractional flow reserve versus angiography for guiding percutaneous coronary intervention. The New England Journal of Medicine 360(3), 213–224 (2009)
18. Truckenbrodt, E.: Fluidmechanik. Springer (1980)
19. Ward-Smith, A.J.: Internal Fluid Flow. Clarendon Press (1980)
20. Westerhof, N., Lankhaar, J.W., Westerhof, B.E.: The arterial windkessel. Medical and Biological Engineering and Computing 47, 131–141 (2009)